Comparison of Above Bandgap Laser and MeV Ion Induced Single Event Transients in High-Speed Si Photonic Devices

Jamie S. Laird[1], Toshio Hirao[2], Shinobu Onoda[2], Hisayoshi Itoh[2], Larry Edmonds[1] and Allan Johnston[1]

Abstract—We illustrate inherent differences between Single Event Transients generated by an above bandgap picosecond lasers and MeV heavy ions by comparing transient currents collected with an ion microbeam and picosecond laser with varying track waist.

I. INTRODUCTION

For some time now, investigating Single Event Effects (SEE) in microelectronics using single photon absorption laser methods has been a successful and cost efficient means [1-4]. Despite the fact that the spatial energy distributions for focused lasers and single ion strikes are quite different, it has generally been accepted that differences in the initial plasma distributions result in second order effects when examining overall transient characteristics. This is quite reasonable for examining processes where the result of the disturbance depends primarily on the amount of charge injected such as a Single Event Upset (SEU) or Single Event Latchup (SEL) and the sensitive region hit is larger than laser track width. Indeed most laser based studies have examined Single Event Transient (SET) propagation in complex devices where the transient response is typically convoluted by a circuit response considerably slower than characteristic charge collection times [5, 6].

Some of the earlier works by McMorrow et al. compared laser induced transients in III-V devices such as GaAs MESFETS [7, 8] to those generated by MeV heavy ions. These results illustrated astonishingly good agreement and surprisingly little dependence on ion track structure. A smaller ion track dependence, although related to accumulated ion damage [9], may also be attributed to the extremely large ambipolar diffusivity in III-V materials where SC effects are known to be reduced [10]. Recent work by the authors of this paper have compared high-injection effects in InGaAs-InP Avalanche Photodiodes (APD)[11] and GaAs Metal Schottky Metal (MSM) photodetectors [10] using a focused MeV ion microbeam with a range of ions designed to give the same end of range but different LET. SC effects were found to be minor on the nanosecond scale compared to those observed in Si devices [12]. In Si devices where the impulse response is transit-time limited, the significantly lower ambipolar mobilities means heavy ions energetic enough to generate high-injection levels produce strong SC screening effects [10, 12-19] which significantly increases charge collection times depending on the ambipolar diffusivity [12, 13, 15]; *even* in a high-field depletion region. These SC effects determine charge collection rates over time scales of increasing importance to SEE in high-speed devices where the circuit response time is similar to the induced current width [9]. In this regime, inherent differences in laser and ion track structures *may* lead to quantitative differences between laser and ion testing. In particular, any significant difference between the two is a particular concern for SET propagation in high-speed devices and may raise some concern when using 1P lasers to *simulate* ion SET related problems including, but not limited to: Bit Error Rate (BER) degradation [20, 21] in sensors and spurious events in optical receivers such as Si *p-i-n* [12, 19] and InGaAs-InP Avalanche Photodiodes [22].

Some authors have attempted to calibrate laser data in complex structures to those of ions by making comparisons with ion data usually collected on a particular location with a microbeam [7, 8]. This process typically involves normalizing the two methodologies based on the total charge collected, which when the same, supposedly implies equivalent effective LET's. This process, while providing a point of reference is fraught with problems, particularly with higher speed devices, situations the laser and ion ranges differ and for device dimensions similar to the laser spot size, where edge effects etc are expected to be significant. It also ignores any Auger recombination, which has a cubic dependence on carrier density and hence more prevalent in ion track structures [9].

More recently, Digital SET propagation in deep submicron control circuitry has been deemed responsible for additional SEU pathways which depend on the initial SET pulse shape [23]. A short SET more readily propagates, eventually latching an SEU further down the combinatorial logic chain. Subtleties in transient current shape have become more important in device operating in the high-frequency or high-clock rate regime, and should be factored in when determining the probability of an SEE pathway.

The research in this paper was carried out at the Jet Propulsion Laboratory, California Institute of Technology under contract with the National Aeronautics and Space Administration (NASA)

[1] California Institute of Technology, Jet Propulsion Laboratory, Pasadena, CA 91109, US

[2] Radiation Effects Group, Department of Severe Environmental Materials, Japan Atomic Energy Agency (JAEA), Takasaki, Gunma, Japan

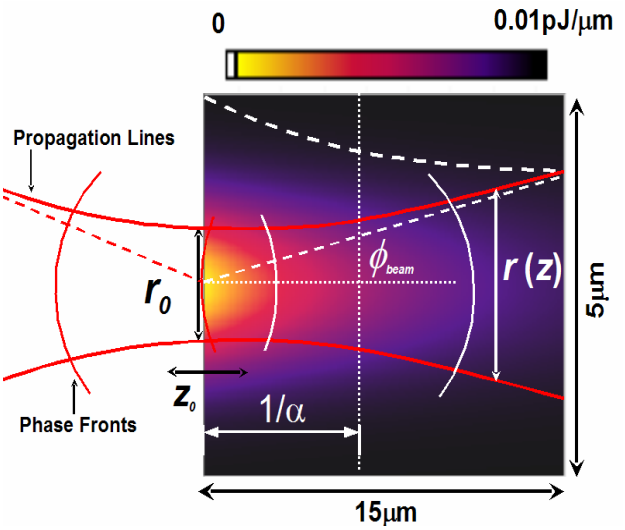

Figure 1: Laser track simulation for a 5μm×15μm Si box for λ=788nm and a surface spot size r_0 of 1.5μm. The energy deposited along the radial dimension is in pJ/μm. While the phase fronts and propagation vectors diverge in the material beyond the confocal depth, exponential absorption results in a funnel shaped generation volume.

As Si remains the material of choice for deep submicron devices and beyond, any difference in ion and laser track structure may lead to differences in SET formation and consequence for examining ultrafast SEE phenomenon such as propagation of SET in combinatorial logic for example. Here we show that these differences can be quite marked when examining fine structure that reveals information on the dynamical high-injection transport parameters. To do so, we examine transient current pulse shapes generated in a *simple* p-n-n^+ epilayer structure by three heavy ions with masses and energies chosen to (a) dump all energy into a fielded region and (b) do so with the same end-of-range which approximately coincides with the absorption length for the laser used. TCAD simulations is used to examine how differences in track parameters such as lateral waist and the longitudinal energy-loss determines overall transient characteristics and under what circumstances ion and laser SET approach one another in Si.

II. HIGH INJECTION EFFECTS AND PLASMA STRUCTURE

As MeV heavy ions pass through materials their energy is primarily lost via electronic stopping which generates a spectrum of free electron energies [24]. As the energy of the ejected electrons is inversely related to ion mass, heavy ions result in narrow track structures than do MeV protons of similar energies. The reduced lateral and depth range of MeV heavy ions result in levels exceeding 10^{18}cm^{-3} over widths less than 100nm [25]. These high-injection (HI) levels result in large SC effects [16, 17] which distort the *E*-field near the ion track thereby altering the transient current shape [26]. Before comparing and discussing measurements, we briefly review calculations of laser and ion track structure with a focus on their radial and longitudinal ranges.

A. *Laser Track Structure*

The optical beam is assumed to be a single mode Gaussian laser which transverses an aberration-less (M^2=1) optical path and focused to a diffraction limited spot at the device surface equal to $r_0 = 4f\lambda/\pi r_l$, where f is the lens focal length and r_l is the beam diameter on the lens. The propagation of the beam as passes through the device media has been described by Yarov, as previously outlined by Melinger et al [3]. The radial profile of the laser intensity at a depth z is:

$$I(r,z) = \frac{2P}{\pi w^2}\exp\left(-2r^2/w(z)^2\right) \qquad (1)$$

where P is the incident laser intensity, r is the radius and w is the Full Width at Half Maximum (FWHM) of the Gaussian distribution which is also depth dependent having the form:

$$w(z) = w_0\left[1+\frac{\lambda z}{\pi w_0{}^2 n}\right]^{1/2} \qquad (2)$$

where n is the refractive index of the material and z_0 is the confocal length $\pi n w_0{}^2/\lambda$ where the beam has expanded by $\sqrt{2}$. As the beam passes through the material it diverges with an angle ϕ_{beam} as indicated in Figure 1. However, for a an above bandgap laser, the intensity of the beam is reduced exponentially in depth by single photon (1P) absorption as described by Beers law [27] with an absorption coefficient, α. For the λ value of 788nm used throughout this work, a Franz-Keldysh absorption shift in high field region can be ruled out [27]. Any Burstein-Moss (BM) shift in the absorption length in the *very* thin p^+ region is also insignificant [27]. The model of Rajkanan et al. [28] using the NASA near-intrinsic Si absorption database was used to estimate α at 300K where all measurements were made. The model of Hawkins et al. was used to interpolate refractive index values [29]. Using the above model an estimated 1/α value was 8μm at λ=788nm. The energy distribution for a laser with a 46ps FWHM Gaussian pulse and r_o value of 1.5μm and peak power of 150mW was calculated as shown in Figure 1 [30].

B. *Ion Track Structure*

Accurately modeling the transient response of a device exposed to MeV ions requires a reasonable estimate of the generated ion track structure since the evolving spatiotemporal response will in part be determined by the initial injection conditions [25, 31]. Here we estimate injection volumes using the method outlined by Kobetich and Katz (KK) which assumes a continuous spectrum of δ–electron energies are generated at each depth [24]. The model predicts an r^{-2} radial distribution where the maximum range r_m is determined by the maximum energy ω_m imparted to δ-electrons given by:

$$\omega_m = \frac{2m_e c^2\beta^2}{1-\beta^2} \qquad (4)$$

where m_e is the electron mass, c is the speed of light and β is the ratio v/c. Algorithms for keV electron energy-loss [30]

are used to calculate the radial energy-loss at each depth and the equality:

$$\frac{dE}{dz} = \int_0^{r_m} D(r)dr \quad (3)$$

normalizes to the energy-loss predicted by SRIM at each depth, *z*. As with the Akkerman, the KK model also predicts $D(r)$ scaling with Z^2_{eff}/β^2 where Z_{eff} is the effective charge of the ion [24]. Unlike the Akkerman model, the KK model overestimates the injection level in the track core resulting in a logarithmic runaway which needs truncating for practical application [32]. They are however, qualitatively correct; that is, the waist of the EHP plasma distribution does increase with ion energy, scale inversely with ion mass and generate HI levels over the order of 10-100nm. Empirical models [33, 34] for the energy required to generate a single *e-h* pair are used to scale $D(r)$ into an EHP plasma distribution, as performed for the three ions (chosen to have the same EOR and β) as displayed in
Figure 2. These ions are 11MeV C, 13MeV N and 15MeV O. Since the volumes and energy-loss profiles are approximately the same, the average injection level is proportional to ion energy.

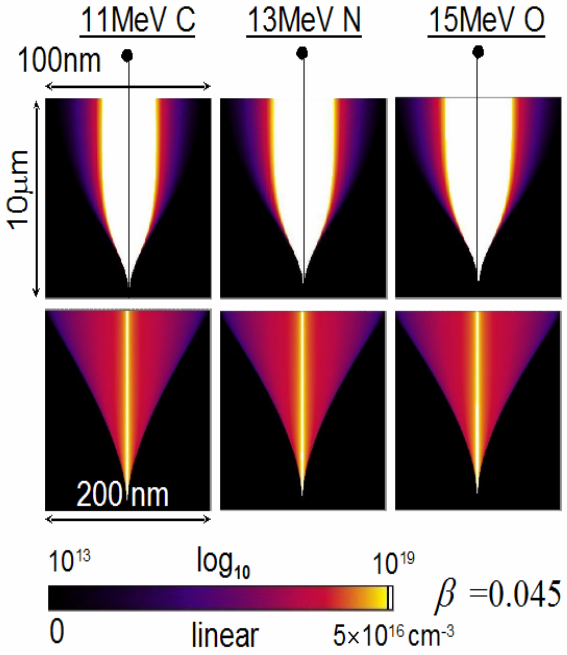

Figure 2: Calculated plasma distributions for 11MeV C, 13MeVN and 15MeV O plot on linear (top) and log (bottom) scales. The tracks waists for all three ions are very similar since all β values are the same. The average plasma density therefore scales with beam energy. Taken from [12].

III. EXPERIMENTAL

A. Device under Test

The device examined here was a 450 μm Si *p-i-n* photodiode used for λ=0.85μm communications with a -3dB BW of f_{-3dB} =1.5GHz at –10V. Shown in Figure 3 is a cross-sectional view of the device indicating its dimensions and equivalent circuit as seen by a load R_L, typically 50Ω. In examining ultrafast transport properties, it is important to reduce the sheet resistance R_{sh} (as well as any series resistance R_s) and device capacitance C_j which result in an intrinsic *RC* pole that lowers f_{-3dB} thereby interfering with the ability to resolve high-speed carrier dynamics. A large substrate doping is therefore a pre-requisite for transit-time limited performance of vertical structures (minimal R_s)

Shown at the bottom of Figure 3 is the dopant profile measured by 4-point probing [35]. The p^+ diffusion extends approximately 1μm into the device with an approximate peak doping of at least 5×10^{18}cm^{-3}. An approximate 10μm near intrinsic region of 2×10^{12}cm^{-3} is followed by an ever increasing rise into the substrate where the dopant level plateaus at 2×10^{18}cm^{-3}. At -20V the device C_j=1.7pF and R_s is dominated by the 50Ω load resulting in a τ_{RC} value of 85ps.

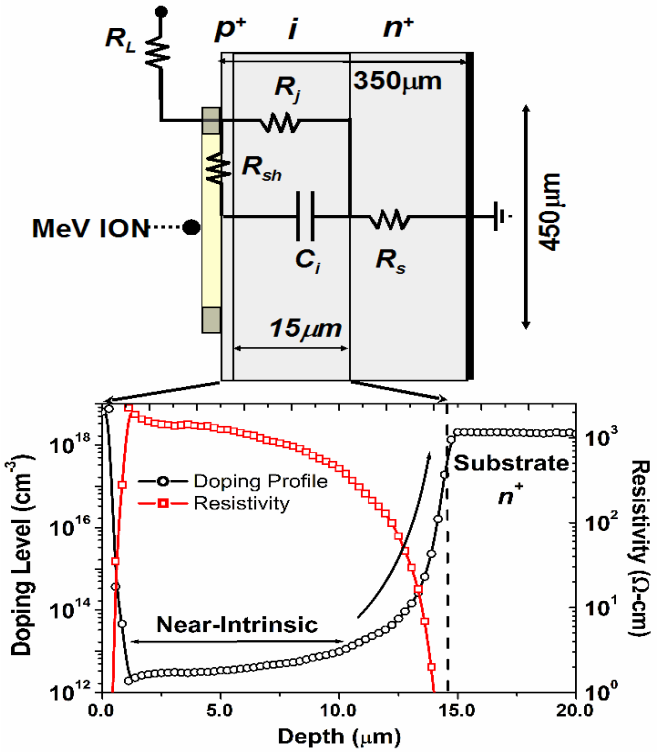

Figure 3: (Top) Equivalent circuit for the p-i-n structure with a load R_L. (Bottom) Dopant profile measured using 4-point spreading resistance.

B. Picosecond Laser System

Both focused picosecond laser and MeV ion microbeam experiments were performed by the Radiation Effects Group at the Japan Atomic Energy Agency (JAEA), Takasaki using the system described elsewhere [36, 37]. Devices were mounted on 50Ω ceramic chip carriers with dual transmission lines carrying the p^+ and ohmic signals to balanced high frequency bias tees. The AC output of both tee's are captured on an external oscilloscope. One of the major differences between the ion and laser configuration is that a 50GHz Tektronix CSA803 was used for all laser work whereas a 3GHz Tektronix TDS694C was used for the case of ions. The risetime of the second system was measured to be 141ps. This difference is not expected to result in any problems when comparing laser and ion SET as differences between the two are largely in the tail of the transient. The total charge generated by the laser pulse was about 1.2pC; 20-30% higher

than that generated by the ions. The laser spot size as measured by scanning the beam across a Metal Semiconductor Metal (MSM) photodetector was approximately 2.7μm [10].

C. Variable Spot Size Laser SET

To examine whether the laser track is capable of generating SC effects to the same degree as a MeV ion of producing approximately the same total charge and range, the DUT to objective lens distance was scanned to adjust the laser waist at the device surface. At each position the average transient current was recorded for a constant dwell time, from which characteristics SET parameters such as peak current and charge were obtained. Shown in Figure 4 are both of these versus Z. At focus (approximately Z=0), screening effects result in a minimum peak current as expected. With increasing $|Z|$ the peak photocurrent increases at higher biases, finally saturating for $|Z|$ >250μm or so. The exponential like drop off after the point r_d denotes the objective position at which the beam spot is approximately the diameter of the device. Beyond r_d carriers are lost due to the laser being reflected by the Al metallization in which case the distribution becomes proportional to Z^{-2}.

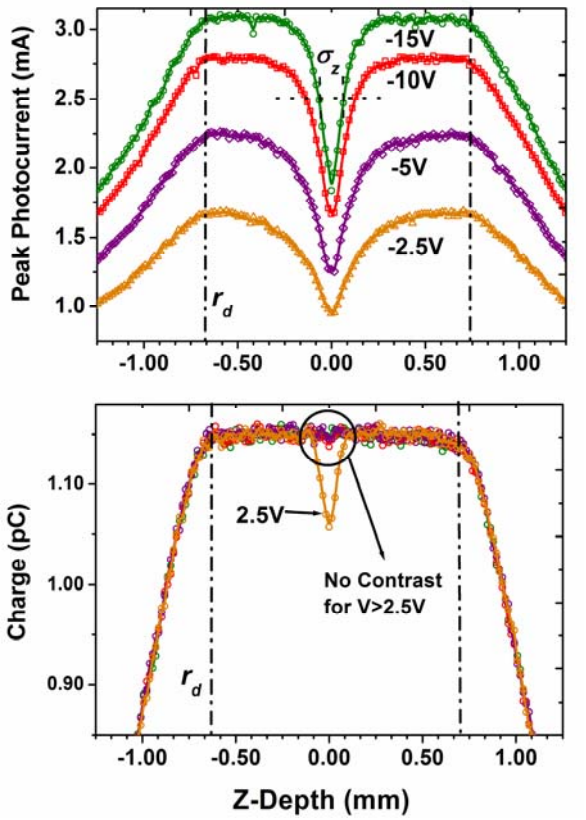

Figure 4: (Top) Peak current vs. z for biases ranging from -2.5V to -15V. (Bottom) Charge vs. Z for the same bias range. All biases bar -2.5V give the same charge up to the point r_d where Auger recombination results in a narrow dip close to focus.

D. Heavy Ion Microbeam SET

The spatial dependence of heavy ion induced SET was collected for 13MeV N, 11MeV C and 15MeV O ions as a function of bias. Images of the device's spatial response (peak current, charge and timing characteristics) were generated and found to be uniform over the central region as described elsewhere [12]. High signal-to-noise ratio (SNR) current transients could then be estimated for each bias by averaging transients over the central region for all three ions, at all biases. These transients together with TP for a broad (Z=500μm) and focused (Z=0μm) laser strike are displayed in Figure 5 for the case of -10V. A log scale is used to highlight the transition between the different charge collection phases.

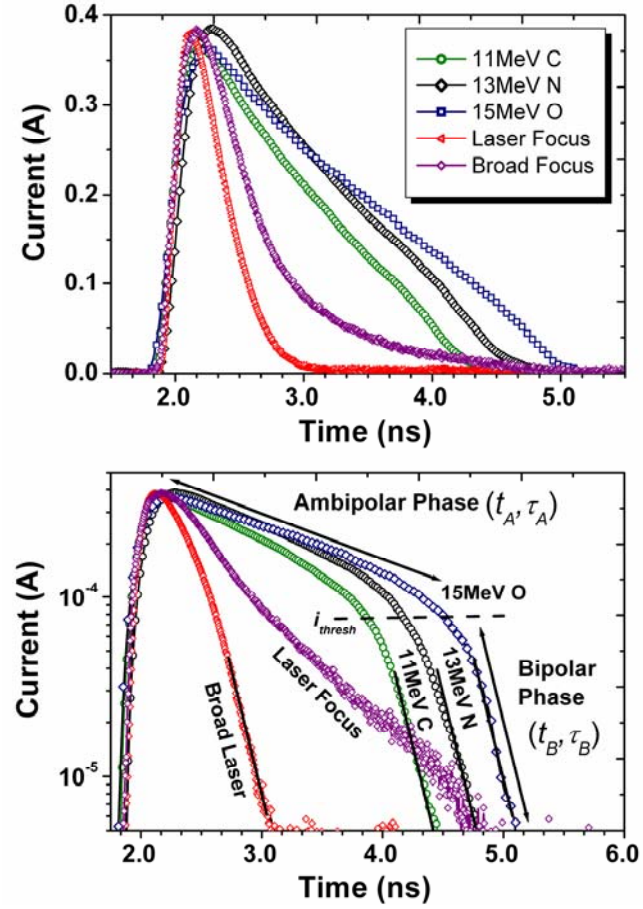

Figure 5: All data was taken at -10V. (Top) Linear-linear plots of the transient current for 11MeV C, 13MeV N and 15meV O, the laser at focus and unfocussed all normalized to the peak current of 11MeV C. (Bottom) Measured SET displayed on a log scale to clearly indicate demarcation in carrier transport phases. In total 5 conditions are displayed including: a "broad" unfocused laser strike, a focused laser strike and all three heavy ions. The ambipolar and bipolar phase durations and gradient are also denoted on the 15MeV O ion SET. The gradient of the bipolar region marked on "broad laser" plots is the same as that for the ions and approximately 1.044mA/ns.

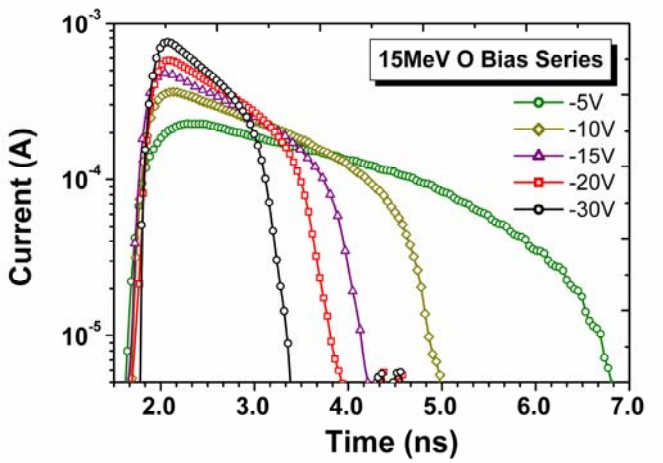

Figure 6: Average transient currents measured as a function of bias for 15MeV O displayed on a log-linear scale. The maximum collection length (the unseen base is actually just below the minimum current threshold shown) is approximately 5ns at -5V and decreases to about 1.6ns at -30V. Note that while the ambipolar period shrinks with bias, the bipolar period remains approximately invariant until a bias of around -5V.

IV. DISCUSSION

A. *TCAD Simulation of High-Injection Space-Charge Screening*

Synopsis TCAD Version 10 with the dopant profile given in Figure 3 was used for all simulations. For more detail on the models and basic assumptions behind the ion simulations, the reader is referred elsewhere [12]. Ion tracks simulated had constant ion track widths of 0.1μm and varying LET's from 0.01pC/μm to 0.2pC/μm. Laser tracks on the other hand has track widths ranging from 0.1μm (for comparison of depth profile alone) to 2μm (for a more realistic simulation). The laser tracks were simulated using an exponential generation with depth profile with an energy which generated the same total charge range as that applied for the ions.

1) *Ion Single Event Transients*

Simulations in this Si *p-n-n*$^+$ structure indicate SC effects result in a large Transient Electric Field (TEF) from the ion end-of-range (EOR) to the *n-n*$^+$ interface [12, 16]. Initially, the plasma negates most of the field from the surface to the EOR resulting in most potential to drop from the EOR to the back n+ interface as shown in the first 100ps or so in FIG 7. This is the so called High Resistance Region (HRR) denoted by Edmonds [16, 17]. Eventually the plasma near the surface erodes by radial ambipolar diffusion and drift and the *E*-field at the surface reappears. With time it gradually extends into the plasma bulk thereby forming a second HRR. Interestingly it does so linearly for the constant carrier profile simulated here. The position of the plasma edges x_{HE} and x_{EE} defining the top and bottom plasma skin is marked on the 400ps image. Both transient fields have amplitudes larger than the maximum of the static *E*-field since the field along most of quasi-neutral column has been largely nullified. The current extracted from the SC screened EHP plasma has a duration which depends on the plasma density via the carrier-density dependence of ambipolar diffusion [12, 16].

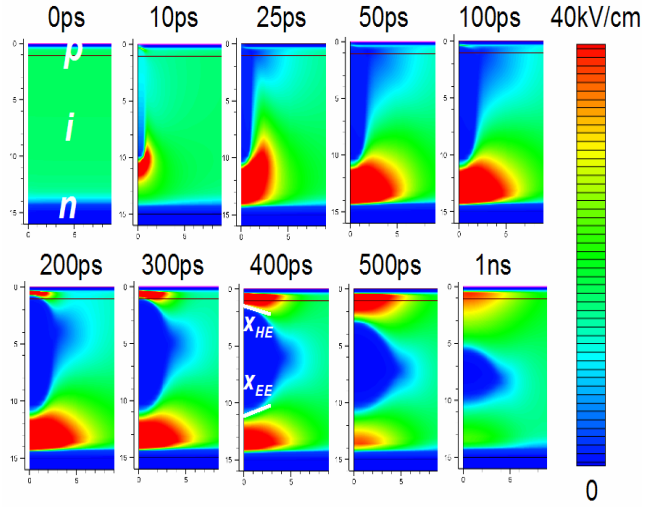

FIG 7: The time-dependence of the absolute value of the TEF from 0 to 1ns for an LET of 0.2pC/μm and -20V bias. Each image is 9μm×16μm. The image at 0ps indicates the static field distribution prior to an ion striking along the left edge. On the far right edge is a linear scale bar from 0 to 40kV/cm. The maximum field is actually higher leading to red saturation. Taken from [12].

Hence the ambipolar phase for the three ions in Figure 5 increases with ion energy. The charge collection time t_c in the simulation agree reasonably well with the measured values displayed in Figure 6. For the case of a laser simulation the situation differs since (a) the laser track has an exponential generation depth profile and (b) has a significantly wider track.

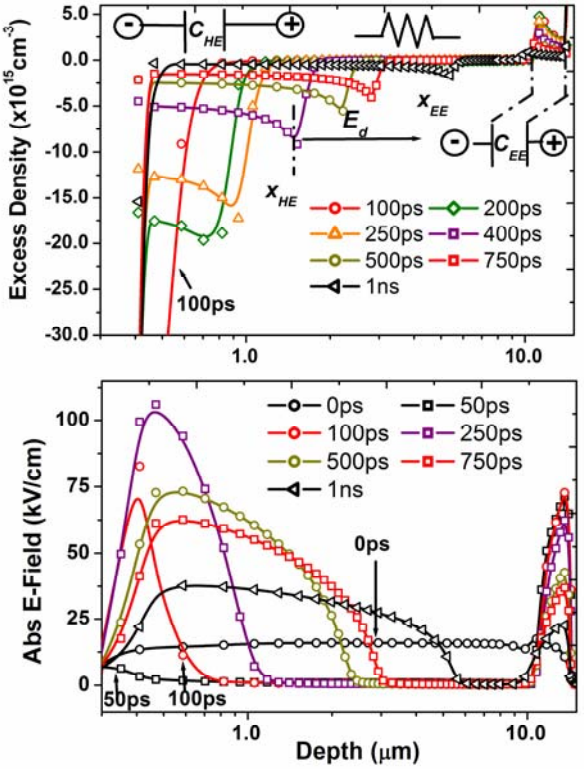

FIG 8: (Top) Plot of the excess EH populations along the center of the ion track from 100ps to 1ns for ρ_{ion}= 0.2pC/μm for a bias of -15V. For short

times the quasi-static charge between x_{HE} and the top electrode forms a transient capacitance C_{HE} which dominates τ_{RC} for this PD geometry and ion trajectory. A resistor is shown to indicate the conductive role of the quasi-neutral plasma. (Bottom) The absolute value of the *E*-field along the same ion track, in this case plotted from 0ps to 1ns. After the ion strike the *E*-field shifts to the back *i*-n^+ interface. Between 50-100ps it begins to recover on the front electrode setting up the bottom HRR.

The above boundary condition leads to the electrode current being approximately twice the minority carrier diffusion current over the period t_A [16]. According to Edmonds, an approximate 1-D expression relating the charge collected in the *A*-phase to the location and density of an ion (or even laser) induced EHP plasma is simply:

$$Q_A(t) = \frac{D_n}{D_A} Q_0 G(D_A t / z_{\max}{}^2) \quad (3)$$

where the function *G* is defined as:

$$G(\zeta) = 1 - \frac{8}{\pi^2} \sum_{n=0}^{\infty} (2n+1)^{-2} \exp\left[-(2n+1)^2 \pi^2 \zeta\right] \quad (4)$$

and z_{max} is the maximum depth of the carrier generation profile [16] which we approximate here as several absorption lengths. In the Boltzmann limit, the ambipolar diffusivity D_A is simply:

$$D_A = \frac{(n+p) D_n D_p}{n D_n + p D_p} \underset{low}{\rightarrow} D_p \underset{high}{\rightarrow} \frac{2 D_n D_p}{D_n + D_p} \quad (5)$$

where *n* and *p* are the electron and hole carrier concentrations and $D_{n,p}$ are the respective electron and hole diffusivities [38]. Under HI conditions the TP is dominated by the *A*-phase which predicts a sum of exponentials whose time-constants (the average of which is τ_A) depends on D_A and α. Increased carrier-carrier scattering at higher injection leads to a decreasing D_A resulting in a slower decay [39].

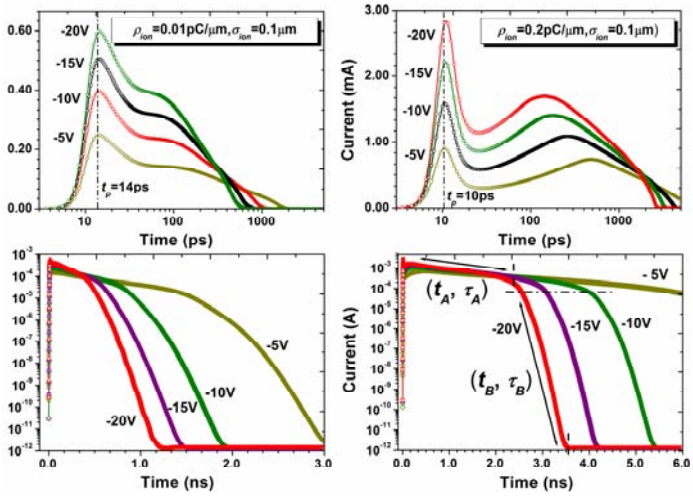

Figure 9: Simulated transient currents for the track geometries representative of the ions used here. The plots on the left shown the bias dependence of an ion with a constant depth-wise LET of 0.01pC/μm whereas the right displays the same results for an ion LET of 0.2pC/μm.

2) Laser Induced Single Event Transients

The laser focus whilst definitely inducing SC effects as noted by the decreased gradient, does not display the stark demarcation between the *A* and *B*-phases seen for ions.. The difference in radius of a around 50 reduces the carrier density by at least several orders of magnitude. Another possibility which really needs simulation for corroboration is the fact that the exponential generation profile of a laser means that the carrier profile rolls off continuously. The stark HRR generated for the ion case may not exist for the laser and carriers can be swept from the back region more efficiently. Possibly, the state of the plasma generated by the focused laser only results in a partial or weakly screening plasma compared to that experienced with ions, even thought the energy deposited is higher, especially near the surface [14].

The rate at which the top HRR moves into the plasma appeared to be linear in simulations; hinting at the fact that with a constant charge depth profile and an escalator like extraction process, the charge collected should almost be linear with time during the ambipolar phase ??. The shape of the transient appears to be similar to the generation shape:

- Is there a bottom HRR for lasers? Initial charge extracted will cause the bottom HRR to be close to the front HRR. Check this with simulation

B. Comparison with III-V Materials

As noted in the introduction, heavy ion transient currents measured in GaAs devices have shown little evidence of larger SC screening effects.

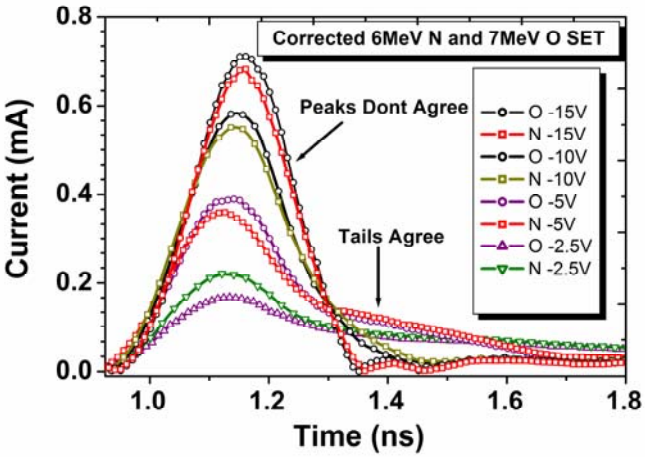

Figure 10: Measured transient currents in a GaAs MSM Schottky barrier for a 6MeV N and 7MeV O beam after correcting for the energy difference. At all biases the transient tails agree remarkably well. At biases beyond reach-trough (~2.5V), the currents differ by around 10% in the peak height. Taken from elsewhere [10]. This was also Auger, but shouldn't the whole transient be smaller not just the peak ??

Not generating a high enough plasma density results in different carrier dynamics dictating the transient current. Furthermore the log scale clearly demarcated two phases of charge collection for the case of ions. These are dictated in time by first the ambipolar and then bipolar drift properties of the plasma. As discussed elsewhere, the duration of the ambipolar phase (denoted by t_A) increases with average LET [12]. However, the bipolar phases with a duration t_B for both ions and laser irradiation have essentially the same

characteristics as realized by similar gradients, τ_B for all four cases.

The lower carrier densities of lasers are expected to shift the laser powers required to observe the clear demarcation noted for ions. However, this raise a wide range of other problems related to the sheer difference in total charge injected, possible heating issue and potential damage if the levels are high enough. In fact, the same problem is likely to occur for 2P probing as well. The Near-Field Optical Microscope (NFOM) is a suitable candidate to both (a) increase the spatial resolution of SEE probing using lasers whilst (b) providing carrier injection profiles similar to that of heavy ions.

V. CONCLUSION

VI. REFERENCES

[1] D. McMorrow, *et al.*, "Picosecond charge-collection dynamics in GaAs MESFETs (for space application)," *IEEE-Transactions-on-Nuclear-Science*, vol. 39, pp. 1657-64, 1992.

[2] A. H. Johnston, "Charge Generation and Collection in p-n Junctions from a Pulsed Infra-Red laser," *IEEE Transactions on Nuclear Science*, vol. 41, pp. 1694 -1702, 1993.

[3] J. S. Melinger, *et al.*, "Critical Evaluation of the Pulsed Laser Methods for Single Event Effects Testing and Fundamental Studies," *IEEE Transactions on Nuclear Science*, vol. 41, pp. 2574-2584, 1994.

[4] S. Buchner, *et al.*, "Confirmation of calculated error rates in a logic circuit using a pulsed laser," presented at Proceedings of 1995 IEEE Nuclear and Space Radiation Effects Conference (NSREC`95). 17-21 July 1995; Madison, WI, USA, 1995.

[5] S. Buchner, *et al.*, "Pulsed laser-induced SEU in integrated circuits: a practical method for hardness assurance testing," *IEEE-Transactions-on-Nuclear-Science*, vol. 37, pp. 1825-31, 1990.

[6] S. Buchner, *et al.*, "Charge collection from focussed picosecond laser pulses," *IEEE-Transactions-on-Nuclear-Science*, vol. 35, pp. 1517-22, 1988.

[7] A. Campbell, *et al.*, "Ion induced charge collection in GaAs MESFETs," *IEEE-Transactions-on-Nuclear-Science*, vol. 36, pp. 2292-9, 1989.

[8] D. McMorrow, *et al.*, "Single-event dynamics of high-performance HBTs and GaAs MESFETs," *IEEE-Transactions-on-Nuclear-Science*, vol. 40, pp. 1858-66, 1993.

[9] D. McMorrow, *et al.*, "Fast charge collection in GaAs MESFETs," *IEEE-Transactions-on-Nuclear-Science*, vol. 37, pp. 1902-8, 1990.

[10] J. S. Laird, *et al.*, "Heavy Ion and Pulsed Laser SET Measurements in High Speed GaAs MSM Photodetectors," *IEEE Transactions on Nuclear Science*, Accepted for Publishing 2005.

[11] J. S. Laird, *et al.*, "Non-linear charge collection mechanisms in high-speed communication avalanche photodiodes," *Nuclear Instruments and Methods in Physics Research Section A: Accelerators, Spectrometers, Detectors and Associated Equipment*, vol. 541, pp. 228-235, 2005.

[12] J. S. Laird, *et al.*, "High-injection carrier dynamics generated by MeV heavy ions impacting high-speed photodetectors," *Journal of Applied Physics*, vol. 98, pp. 013530, 2005.

[13] P. A. Tove, *et al.*, "Plasma Effects in Semiconductor Detectors," *Nuclear Instruments and Methods in Physics Research*, vol. 51, pp. 261-269, 1967.

[14] P. A. Tove, *et al.*, "Recombination in light-pulse excited silicon at medium-high carrier concentration levels," *Journal of Applied Physics*, vol. 44, pp. 2690-2692, 1973.

[15] W. Seibt, *et al.*, "Charge Collection in Silicon Detectors for Strongly Ionizing Particles," *Nuclear Instruments and Methods in Physics Research*, vol. 113, pp. 317-324, 1973.

[16] L. D. Edmonds, "Charge Collection from Ion Tracks in Simple Epi Diodes," *IEEE Transactions on Nuclear Science*, vol. 44, pp. 1448, 1997.

[17] L. D. Edmonds, "Electric Currents Through Ion Tracks In Silicon Devices," *IEEE Transactions on Nuclear Science*, vol. 45, pp. 3153, 1998.

[18] V. Ferlet-Cavrois, *et al.*, "Charge collection by capacitive influence through isolation oxides," *IEEE Transactions on Nuclear Science*, vol. 50, pp. 2208-2218, 2003.

[19] J. S. Laird, *et al.*, "The Role of High-Injection Effects on the Transient Ion Beam Induced Current Response of High-Speed Photodetectors," *Nuclear Instruments and Methods in Physics Research Section B: Beam Interactions with Materials and Atoms*, vol. 219-220, pp. 1015-1021, 2004.

[20] P. Marshall, *et al.*, "Charged particle effects on optoelectronic devices and bit error rate measurements on 400 Mbps fiber based data links," *IEEE Transactions on Nuclear Science*, vol. 41, pp. 528-533, 1994.

[21] P. W. Marshall, *et al.*, "Single event effects in circuit-hardened SiGe HBT logic at gigabit per second data rates," *IEEE-Transactions-on-Nuclear-Science*, vol. 47, pp. 2669-74, 2000.

[22] J. S. Laird, *et al.*, "Heavy-ion induced single-event transients in high-speed InP-InGaAs avalanche photodiodes," *IEEE Transactions on Nuclear Science*, vol. 50, pp. 2225-2232, 2003.

[23] J. Benedetto, *et al.*, "Heavy ion-induced digital single-event transients in deep submicron Processes," *Nuclear Science, IEEE Transactions on*, vol. 51, pp. 3480-3485, 2004.

[24] E. J. Kobetich, *et al.*, "Energy Deposition by Electron Beams and δ rays," *Physical Review*, vol. 170, pp. 391, 1968.

[25] W. J. Stapor, *et al.*, "Charge collection in silicon for ions of different energy but same linear energy transfer (LET)," *Nuclear Science, IEEE Transactions on*, vol. 35, pp. 1585-1590, 1988.

[26] R. S. Wagner, *et al.*, "Alpha-, Borob-, Silicon- and Iron- Ion-Induced Current Transients in Low-Capacitance Silicon and GaAs Diodes," *IEEE Transactions on Nuclear Science*, vol. NS-35, pp. 1578-1584, 1988.

[27] J. Pankove, *Optical Processes in Semiconductors*. New York, 1975.

[28] K. Rajkanan, *et al.*, "Absorption coefficient of silicon for solar cell calculations," 1979.

[29] G. Hawkins, "Spectral Characterisation of Infrared Optical Materials and Filters," in *Department of Cybernetics*: Reading University, 1998.

[30] T. Tabata, "A Simple Calculation for Mean Projected Range of Fast Electrons," *Journal of Applied Physics*, vol. 39, pp. 5342-5343, 1968.

[31] H. Dussault, *et al.*, "The effects of ion track structure in simulating single event phenomena," presented at Radiation and its Effects on Components and Systems, 1993.,RADECS 93., Second European Conference on, 1993.

[32] A. Akkerman, *et al.*, "Ion Track Structure and its Effect in Small Size Volumes of Silicon," *IEEE Transactions on Nuclear Science*, vol. 49, pp. 3022, 2002.

[33] C. Klein, "Bandgap Dependence and related Features of Radiation Ionization Energies in Semiconductors," *Journal of Applied Physics*, vol. 39, pp. 2029, 1968.

[34] R. C. Alig, *et al.*, "Electron-hole-pair creation energies in semiconductors," *Physical Review Letters*, vol. 35, pp. 1522-1525, 1975.

[35] P. Blood, *et al.*, *The Electrical Characterisation of Semiconductors: Majority Carrier and Electron States*, vol. 13: Academic Press, 1992.

[36] I. Nashiyama, *et al.*, "Single Event Current Transients Induced By High Energy Ion Microbeams," *IEEE Transactions on Nuclear Science*, vol. 40, pp. 935, 1993.

[37] J. S. Laird, *et al.*, "Development of a new data collection system and chamber for microbeam and laser investigations of single event phenomena," *Nuclear Instruments and Methods in Physics Research Section B: Beam Interactions with Materials and Atoms*, vol. 181, pp. 87-94, 2001.

[38] J. P. McKelvey, *Solid State and Semiconductor Physics*. Florida: Krieger Publishing, 1986.

[39] S. Tiwari, *et al.*, "On the role of mobility and saturated velocity in the dynamic operation of p-i-n and metal-semiconductor-metal photodetectors," *Applied Physics Letters*, vol. 60, pp. 1135-1137, 1992.